Identification of Cinnamic Acid Derivatives As Novel Antagonists of the Prokaryotic Proton-Gated Ion Channel GLIC

Marie S. Prevost,[†,‡,§] Sandrine Delarue-Cochin,[‖,⊥] Justine Marteaux,[‖,⊥] Claire Colas,[#,▽] Catherine Van Renterghem,[†,‡] Arnaud Blondel,[#,▽] Thérèse Malliavin,*[,#,▽] Pierre-Jean Corringer,*[,†,‡] and Delphine Joseph*[,‖,⊥]

[†]Institut Pasteur, Unité Récepteurs-Canaux, Paris, France

[‡]CNRS UMR 3571, Paris, France

[§]Université Pierre et Marie Curie (UPMC), Cellule Pasteur, Paris, France

[‖]Université Paris-Sud, Équipe de Chimie des Substances Naturelles, Châtenay-Malabry, France

[⊥]CNRS UMR 8076 BioCIS, Châtenay-Malabry, France

[#]Institut Pasteur, Unité de Bioinformatique Structurale, Paris, France

[▽]CNRS UMR 3528, Paris, France

S *Supporting Information*

ABSTRACT: Pentameric ligand gated ion channels (pLGICs) mediate signal transduction. The binding of an extracellular ligand is coupled to the transmembrane channel opening. So far, all known agonists bind at the interface between subunits in a topologically conserved "orthosteric site" whose amino acid composition defines the pharmacological specificity of pLGIC subtypes. A striking exception is the bacterial proton-activated GLIC protein, exhibiting an uncommon orthosteric binding site in terms of sequence and local architecture. Among a library of *Gloeobacter violaceus* metabolites, we identified a series of cinnamic acid derivatives, which antagonize the GLIC proton-elicited response. Structure−activity analysis shows a key contribution of the

carboxylate moiety to GLIC inhibition. Molecular docking coupled to site-directed mutagenesis support that the binding pocket is located below the classical orthosteric site. These antagonists provide new tools to modulate conformation of GLIC, currently used as a prototypic pLGIC, and opens new avenues to study the signal transduction mechanism.
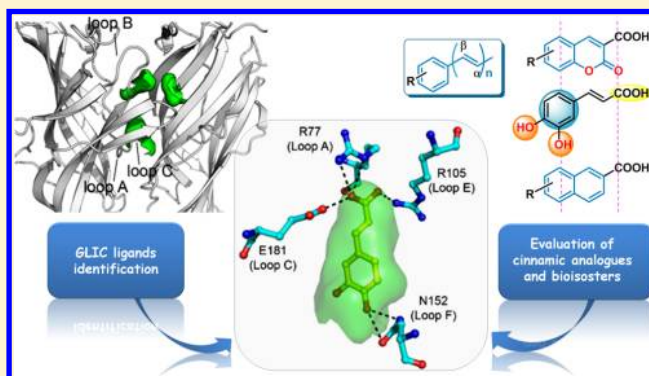
INTRODUCTION

Pentameric ligand gated ion channels (pLGICs) mediate signal transduction by binding agonists, typically neurotransmitters, within their extracellular domain (ECD) coupled to a global allosteric reorganization, leading to ion channel opening within their transmembrane domain (TMD).[1] So far, pLGICs were found in animals, including vertebrates and invertebrates, as well as in several bacteria and a single archea.[2] Thus, pLGICs constitute a large superfamily of receptors that are activated by a wide range of small organic compounds, notably the neurotransmitters acetylcholine (activating nicotinic acetylcholine receptors, nAChRs), glycine (activating the GlyRs), glutamate (activating notably the glutamate chloride channel GluCl from *Caenorhabditis elegans*), γ-aminobutyric acid (activating the GABA_ARs), and serotonin (activating the 5-HT_3Rs), but also by zinc and protons. Despite this large diversity in chemical structures, the wealth of biochemical and structural data accumulated over the past decades show that all these agonists, except protons and zinc, mediate their effect through the binding to a topologically conserved site from bacteria to human: the orthosteric binding site.[1]

Initially studied by photoaffinity labeling and mutagenesis, the X-ray data accumulated over the past decade provide a better 3D picture of the orthosteric binding site. For instance, GluCl was cocrystallized with glutamate, its agonist,[3] and the bacterial pLGIC from *Erwinia chrysanthemi* ELIC was cocrystallized with bromopropylamine,[4] one of its agonists, and with acetylcholine,[5] one of its antagonists (Figure 1). Furthermore, AChBPs, soluble nAChRs homologues of the ECD, were cocrystallized with diverse agonists and antagonists, thus providing a wide corpus of structural information.[6] The orthosteric site is located within the ECD at the interface between subunits, halfway between the ECD apex and the membrane.[1] It is formed by the A-, B-, and C-loops from one subunit (principal component) and the D-, E-, F-, and G-loops
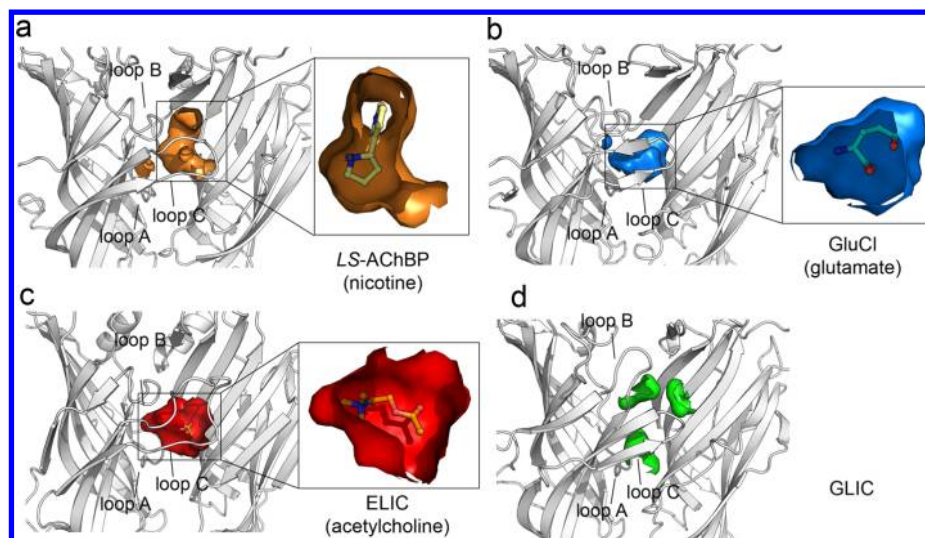
Figure 1. High-resolution structures of orthosteric binding sites of pLGICs. Structures are represented in cartoon as a dimer of extracellular domains (Ls-AChBP in complex with nicotine ((a) PDB entry 1UW6), GluCl with glutamate ((b) PDB entry 3RIF), ELIC with acetylcholine ((c) PDB entry 3RQW), and GLIC ((d) PDB entry 3EAM)), the cavities calculated by PyMol and lined by atoms within 5 Å of the ligand are shown in surface. For GLIC, atoms within 5 Å of nicotine, glutamate, and acetylcholine molecules when all the four structures are superimposed were selected.

from the next subunit (complementary component), where E- and D- "loops" are in fact involved in adjacent β-strands and not from per se loop structures. Extensive studies on AChBPs and nAChRs showed that, for those receptors, A-, B-, C-, and D-loops bring in Trp, Tyr, or Phe residues. One of the aromatic residues forming the aromatic box comes from D-loop from the complementary site of the interface. A systematic mutational analysis further corroborated a key role for the B-loop in nAChRs, in which a Trp elicits direct cation−π interaction with the ammonium ion.[7] Similarly, A-, B-, and C-loops of GluCl and ELIC bring in several aromatic residues for the binding of the primary ammonium of bromopropylamine (ELIC) and glutamate (GluCl). Site-directed mutagenesis studies showed that equivalent features are conserved in the GABA$_A$, glycine, and 5-HT$_3$ receptors.[8−10] The remaining parts of the orthosteric site appears more variable, accounting for the pharmacological diversity of pLGIC subtypes.

The bacterial homologue GLIC from *Gloeobacter violaceus*, whose structure is the highest resolved among pLGICs (first at 2.9 Å[11] then at 2.4 Å[12]), provides a strikingly different picture. Indeed, we showed that GLIC is activated by protons and so far no organic agonist targeting GLIC have been described.[13] Nevertheless, we recently showed that not only GLIC but also a chimera composed of the ECD of GLIC fused to the TMD of the α1GlyR are activated by protons, showing that the proton activation site(s), although not identified precisely, is (are) carried by the ECD.[14] Furthermore, the orthosteric site of GLIC constitutes an outlier within the pLGIC family both in terms of amino acid composition and of local conformation: (i) it carries a cluster of charged residues and not of aromatic residues facing the orthosteric site at the level of the binding loops (Supporting Information Figure 1) and (ii) the local conformation of the B-loop adopts an atypical upward extended conformation as compared to its highly conserved topology in all other pLGICs solved by X-ray crystallography. In addition, the orthosteric agonist-binding cavity itself, visible for the other members, is absent in GLIC, notably due to an arginine of the B-loop which overlaps with the ligands when GLIC structure is superimposed on those of ELIC, AChBP, or GluCl, and to a

tight "clamp" of the C-loop. Thus, facing to other pLGICs, the GLIC "orthosteric" site is atypical, implicating that the ligand binding site in this region could be also unusual.

Because the X-ray crystallographic structure of GLIC has been solved at the highest resolution (2.8 Å at the start of our study), this protein is particularly suitable for rational in silico ligand binding studies. With the aim of discovering ligands binding to the orphan orthosteric site of GLIC, we combined in silico screening, electrophysiological recording, and chemical synthesis. We screened a library of compounds involved in the metabolism of *G. violaceus* that allowed the development of the first series of cinnamic acid derivatives that inhibit GLIC currents at a micromolar range.

RESULTS

Initial Identification of GLIC Ligands Using a Library of *Gloeobacter violaceus* Metabolites. In the ligand-bound structures of ELIC, GluCl, and AChBPs, relatively large binding pockets are observed at the orthosteric site (Figure 1a−c), with a calculated volume ranging from 330 to 540 Å^3 (defining the cavity as the empty volume distant from the bound ligand by less than 5 Å, all volumes were calculated using HOLLOW (http://hollow.sourceforge.net),[15] and the smallest ligands, such as amino acids, are about 150 Å^3 large. On the contrary, in the GLIC structure, Arg133 from the B-loop together with the capped conformation of the C-loop fill almost completely the central part of the interface, producing three independent smaller pockets in the apical and basal sides of the interface (Figure 1d). Those pockets, while small (calculated volumes of 70, 90, and 180 Å^3), may still receive ligands having the size of neurotransmitters (Figure 1d) if extended farther than 5 Å.

For in silico docking, we selected a list of 2736 low-molecular-weight compounds that are described in the Kyoto Encyclopedia of Genes and Genomes (KEGG (http://www.genome.jp/kegg/)) database as being involved in the *Gloeobacter violaceus* metabolic and regulatory pathways. Indeed, our electrophysiological assays do not allow high throughput experiments. The 3D structures of compounds with

Table 1. Activity of the Cinnamic Acid Derivatives and Analogues[a]

compd	IC$_{50}$ ± SD (at pH 5.5)	n_H (Hill number)	pK_a***	maximal inhibition at 1 mM (% ± SD)	no. of cells
Cin-COOH	34.6 ± 6.0 μM	1.0 ± 0.1	4.45	97.5 ± 0.2	3
3-Cl-Cin-COOH	13.7 ± 0.9 μM	0.9 ± 0.05	4.8	95 ± 1.9	3
3-CF$_3$-Cin-COOH	25.3 ± 1.4 μM	1.1 ± 0.06	4.6	94.6 ± 2.1	3
4-OH-Cin-COOH	9.59 ± 1.7 μM	0.64 ± 0.08	ND	91.4 ± 5.6*	3
3,4-OCH$_2$O-Cin-COOH	28.8 ± 1.4 μM	1.1 ± 0.06	ND	79.7 ± 5.5**	3
Cin-CONHOMe	ND	ND		ND	3
Cin-(COOH)$_2$	7.94 ± 4.8 mM	0.6 ± 0.1	3.5/4.95	25.0 ± 9.5	3
Cin-CH=C(COOH)$_2$	83.5 ± 5.4 μM	0.9 ± 0.05	3.45/6.0	92.2 ± 2.3	3
α-H-β-oxa-Cin-COOH	53.3 ± 2.5 μM	1.3 ± 0.07	3.2	98.5 ± 0.5	3
α-OH-β-H-Cin-COOH	ND	ND	ND	ND	3
Cin-CN	ND	ND		ND	3
Caf-COOH	16.7 ± 1.2 μM	0.9 ± 0.05	4.35	93.76 ± 1.2	6
4-O-Me-Caf-COOH	13.5 ± 1.3 μM	0.8 ± 0.06	ND	98.5 ± 0.5	3
Caf-CH$_2$-OH	73.9 ± 7.7 μM	1.4 ± 0.2		95.2 ± 1.1	3
Caf-COOEt	246 ± 46 μM	1.3 ± 0.3		91.8 ± 4.4	3
Caf-COOMe	388 ± 67 μM	1.1 ± 0.2		78.0 ± 7.2	3
Caf-CONH$_2$	347 ± 90 μM	0.6 ± 0.1		51.6 ± 3.1*	3
Caf-CONHEt	295 ± 66 μM	1.0 ± 0.2		81.6 ± 2.1	3
α,β-diH-Caf-COOH	86.8 ± 5.2 μM	0.9 ± 0.04	4.30	90.5 ± 2.2	3
3,4-diO-Me-Caf-COOH	206 ± 21 μM	0.97 ± 0.1	4.55	75.6 ± 2.4	3
Napht-COOH	61.4 ± 7.9 μM	1.1 ± 0.1	4.45	96.4 ± 0.8	3
Napht-SO$_3$H	ND	ND	ND	ND	3
Coum-COOH	282 ± 20 μM	1.2 ± 0.1	3.60	84.0 ± 9.3	3
7-OMe-Coum-COOH	168 ± 14 μM	1.4 ± 0.1	ND	96.0 ± 3.5	3

[a]For solubility issues, some compounds were tested up to 300 μM (*) or 100 μM (**). For some compounds, pK_a were measured for a 1 mM aqueous solution containing 1% of DMSO (***).

their hydrogen atoms and their charges were calculated using Corina[16] and qpd.[17]

To find initial hits by in silico screening, we chose in a first attempt to artificially enlarge the cavity. For that, we chose to produce a model of GLIC where the C-loop, known to be flexible from the various AChBP structures, is forced in an open conformation through its alignment on the nicotine-bound AChBP's C-loop conformation (PDB 1UW6), using Modeler (data not shown).[18] Compounds were then docked on homology models using FlexX 2.2.[19] Among the best scores, 46 compounds were finally manually selected based on the poses redundancy, reasonable size, and polar properties to be experimentally tested on GLIC.

Caffeic Acid Inhibits Proton-Elicited Currents with Micromolar Affinity. As compounds available in the KEGG database are not related to any real compound library and cover as well a large structural diversity, we were faced with the problem of synthesizing or ordering the compounds with best scores. To overcome this difficulty, the InChiKeys[20] (The IUPAC International Chemical Identifier (InChI), IUPA, 5 September 2007) of the 46 selected compounds were determined. These compounds were then identified in the French "Chimiothèque Nationale" (http://chimiotheque-nationale.enscm.fr/) and were tested for their effect on the GLIC protein using two-electrode voltage-clamp electro-physiology upon expression in *Xenopus* oocytes.

For the initial screening, we selected a procedure allowing identification of both potentiating and inhibiting compounds: oocytes expressing GLIC were first challenged with a pH 5.5 MES-solution (near the EC$_{50}$ of GLIC activation) during 30 s, a period sufficient to reach a steady-state current. Then the compounds were applied for 30 s at a 0.1 mg/mL concentration (which gives an approximated 0.5 mM

concentration depending on the molecular weight of the compounds) in the same pH 5.5 buffer. Finally, the compounds were washed away with pH 5.5 buffer alone to check the reversibility of their effect. Only two compounds modified GLIC currents: even if the rank of these two ligands was respectively 17 and 20 within the 46 potentially agonists initially selected, with corresponding FlexX scores of −26.50 and −25.77, caffeic acid, and 2-hydroxycinnamic acid inhibited GLIC currents at micromolar concentrations when coapplied with protons. While the two active compounds are very close in terms of chemical structure, the caffeic acid was slightly more potent and was thus selected for further characterization. The 44 remaining selected compounds had no effect and were excluded for further analysis. Even if this approach yielded active compounds, the relatively low proportion of active compounds obtained from the initial docking questions the relevance of the artificially cavity-enlarged model to describe the interaction with orthosteric ligands. To be more realistic, the intact GLIC structure will be used as a better model to interpret the whole set of data and the initial GLIC model was abandoned for further analysis.

The dose−response curve for the inhibition of pH 5.5-elicited GLIC currents by caffeic acid shows that the current is decreased by 93.7% at the saturating concentration of 1 mM with an IC$_{50}$ at 16.7 ± 1.2 μM (Table 1). This inhibition is reversible upon washing and is not modified by a change of voltage (data not shown), excluding a channel-block effect, because caffeic acid is mainly deprotonated and therefore charged at this pH (pK_a = 4.65).

Synthesis of Cinnamic Acid Analogues. With the ambition to define pharmacophores implied in the inhibiting activity and to identify novel more potent and/or more efficient potential ligands, we undertook a systematic structure−activity
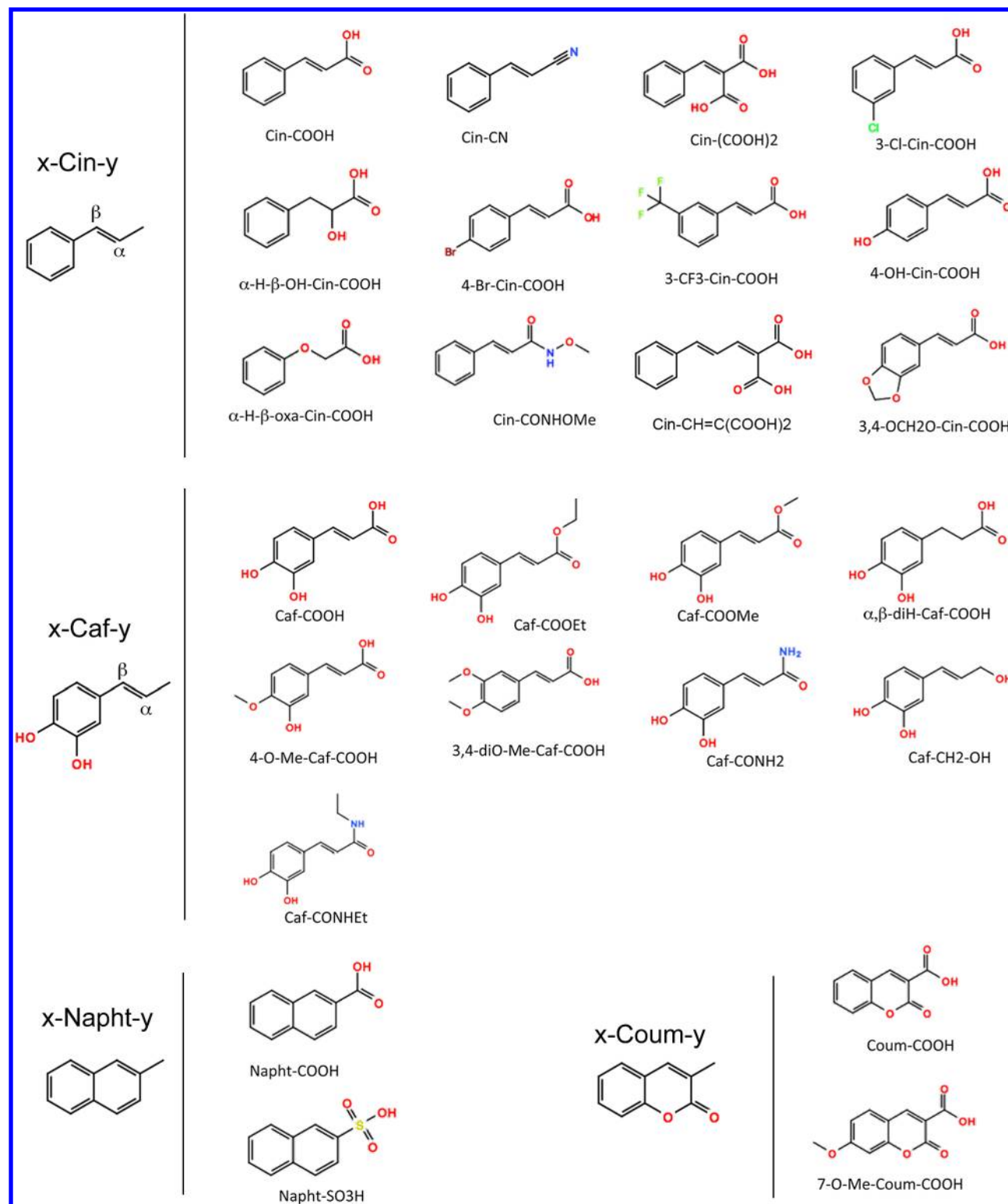
Figure 2. Evaluated compounds and nomenclature adopted.

analysis by introducing chemical modifications on the three functional parts of the caffeic scaffold: (i) the catechol moiety, (ii) the terminal carboxylate function, and (iii) the ethylenic spacer.

A series of synthesized or commercially available compounds were elected for their similar general shape derived from the cinnamic platform with a western aromatic part linked to an eastern terminal function by at least two carbon atoms. To

clearly visualize the pharmacomodulations introduced, we adapted the compounds nomenclature in relation with its carbon skeleton nature (Figure 2).

We distinguished four different scaffold series: (i) analogous to caffeic acid, the 3,4-dihydroxylated styrene framework (named as **x-Caf-y**), (ii) equivalent to cinnamic acid, the variously substituted styrene skeleton (**x-Cin-y**), and in order to
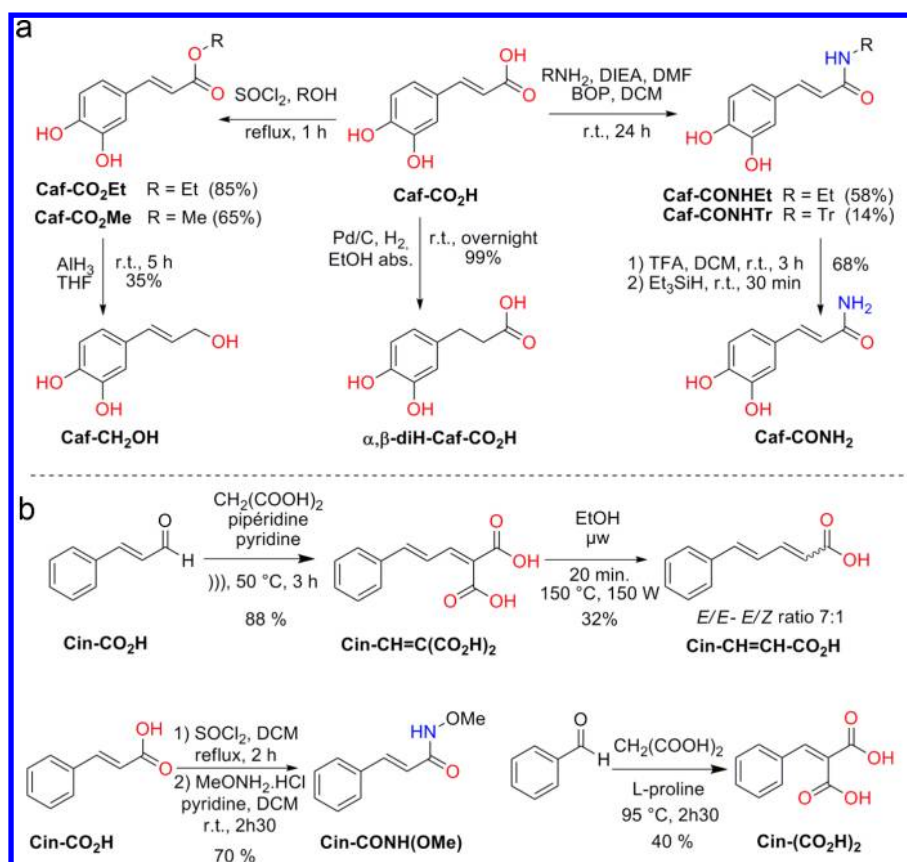
Figure 3. Access to synthetic ligands of the caffeic (a) and cinnamic (b) series.
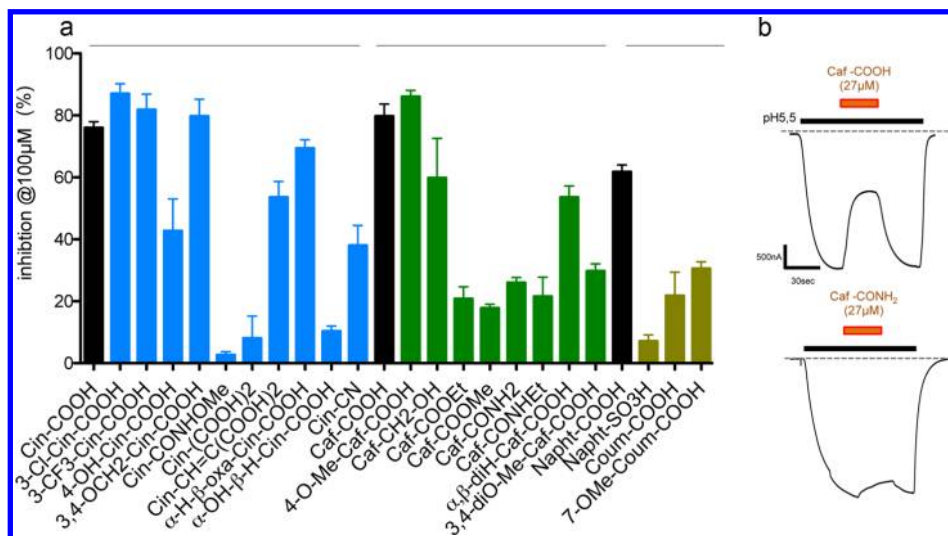

Figure 4. Activities of the caffeic acid analogues. (a) Inhibition of GLIC currents at pH 5.5 by a 100 μM compound solution. (b) Example traces of current inhibition by coapplication of protons and **Caf-COOH** or **Caf-CONH$_2$**.

develop new fluorescent ligands, (iii) the naphthalene (**x-Napht-y**) and (iv) coumarin (**x-Coum-y**) platforms (Figure 2).

Concerning synthetic ligands of caffeic series (**x-Caf-y**; Figure 3a), standard procedures of esterification[21] and amidation[22] of caffeic acid (**Caf-CO$_2$H**) afforded in relatively good yields the methyl and ethyl caffeates (**Caf-CO$_2$Me** and **Caf-CO$_2$Et**) and the amide derivative **Caf-CONHEt**, respectively. The primary amide **Caf-CONH$_2$** was prepared according to a two-step procedure using tritylamine as a synthetic equivalent of ammonia.[23] Finally, the dihydrocaffeic acid (**α,β-**

diH-Caf-CO$_2$H) was obtained by catalytic hydrogenation of caffeic acid. Reduction of methyl caffeate **Caf-CO$_2$Me** by in situ prepared AlH$_3$[24] led to alcohol derivative **Caf-CH$_2$OH** in modest yield.

In the case of synthetic ligands of cinnamic series (**x-Cin-y**; Figure 3b), we were interested in preparing cinnamic acid analogues in which the carboxylic acid function was modified. N-Methoxy cinnamamide **Cin-CONH(OMe)** was synthesized in a good 70% yield over two steps from cinnamic acid.[25] In addition, the Knoevenagel condensation of benzaldehyde with

malonic acid using L-proline as both solvent and organocatalyst afforded the diacid analogue **Cin-(COOH)$_2$** in moderate 40% yield.[26]

To study the effect of the molecule length on ligand activity and affinity, we attempted to prepare the vinylogous cinnamic acid **Cin-CH=CH-CO$_2$H**. Its access was quite difficult. Indeed, Knoevenagel–Doedner condensation of cinnamaldehyde with malonic acid in standard conditions under ultrasound activation did not give the expected adduct.

The Knoevenagel vinylogous α-carboxycinnamic acid **Cin-CH=C(COOH)$_2$** was the sole isolated compound in high 90% yield. In a second step, the diacid decarboxylation was carried out under microwave irradiation, giving a mixture of two separable stereoisomers in a 7:1 ratio in favor of the E/E isomer which was isolated in 28% yield.

A total of 15 commercial and nine synthetic compounds were thus used for further analysis (Figure 4 and Table 1).

The Carboxylate Moiety Is Determinant for the Inhibitory Effect. Both commercial and synthetic derivatives were tested in *Xenopus* oocytes expressing GLIC WT at pH 5.5, with the same protocol that was used for the initial screening of the caffeic acid (Figure 4, Table 1).

Concerning the variation of phenyl substituents on **Cin-COOH** or **Caf-COOH** scaffold, results showed that the nature of the weak deactivating atom or function, positioned in *meta* and/or *para* of the unsaturated arm, had moderate effects on the compound's activity (change in IC$_{50}$ less than 3-fold). Nevertheless, steric hindrance of the conjugate acid imposed by the presence of a methoxy group in position *meta* (**3,4-diOMe-Cin-COOH**, 12-fold increase in IC$_{50}$) results in an erosion of the corresponding ligand activity.

Furthermore, replacement of the deprotonable carboxylic acid function by analogous proton-donating amide groups (**Cin-CONHOMe**, **Caf-CONH$_2$**, and **Caf-CONHEt**) or analogous proton-accepting ester functions (**Caf-CO$_2$Et** and **Caf-CO$_2$Et**) resulted in a marked decrease of the inhibitory activity (more than a 100-fold change in IC$_{50}$). Converting the cinnamic acid into hindered benzylidenemalonic acid (**Cin-(COOH)$_2$**) causes a complete loss of activity. Conversely, reduction of the carboxylic acid group into the more flexible H-bond accepting alcohol function (**Caf-CH$_2$OH**) maintains a good activity.

Finally, structure–activity relationship studies were extended to evaluate the effect of the linker nature between the aromatic part and acidic function. Modification of the *trans*-acrylic acid region by the analogous hydrogenated propionic acid (**α,β-diH-Caf-COOH**) or by the bioisosteric oxyacetic acid (**α-H,β-oxa-Cin-COOH**) has a slight but significant decrease in inhibitory effect: the presence of an unsaturated linker able to delocalize with the π-system improves potency over the simple CH$_2$–CH$_2$ linker element (**α,β-diH-Caf-COOH**). These results showed the importance of the rigid and planar conformation adopted by this linking part to maintain the inhibiting activity. Similarly, replacement of styrene moiety by naphthalene as constraint isoelectronic analogue (**Napht-COOH**) gives more or less the same compound activity, confirming the importance of the planar structure. Nevertheless, as expected according to the weaker potency of the hindered **Cin-(COOH)$_2$**, coumarin analogue (**Coum-COOH**) exhibits an 8-fold lower potency than the cinnamic acid (**Cin-COOH**). Surprisingly, elongation of the acrylic linker into an acrylic vinylogue (**Cin-CH=C(COOH)$_2$**) favors the recovering of a good activity (2.5-fold inferior to **Cin-COOH**).

Notice that the more acidic naphthalene-2-sulfonic analogue (**Napht-SO$_3$H**), the cinnamonitrile analogue (**Cin-CN**), the **Cin-CONHOMe** analogue and the hydrogenated cinnamic acid bearing a proton-donating group in α position (**α-OH,β-H-Cin-COOH**) have no significant effect on GLIC currents up to 1 mM.

Moreover, as the carboxylic function seems to play an important role in the compounds activity. We studied how the deprotonation propensity of these carboxylic derivatives can affect their activity, and pK_a of chosen compounds have been measured (Table 1).

The pK_a range of these weak monoacids is comprised between 3.2 and 4.8, suggesting that at pH 5.5, the carboxylic derivatives are in their deprotonation state, justifying why amide and ester derivatives bearing lesser proton-accepting functions are fewer potent than their carboxylic acid analogues. Moreover, the nature of the hydrophobic part seems to slightly influence the pK_a variations, that is, in coherence with the similar activity observed for the **Cin-COOH** and **Caf-COOH** series. In addition, although **Coum-COOH** and **α-H-β-oxa-Cin-COOH** are in the same range of pK_a, **α-H-β-oxa-Cin-COOH** is 5.3-fold more inhibiting than **Coum-COOH**, confirming the deleterious effect of the stereoelectronic hindrance of the carboxylic function.

In summary, engineering the catechol moiety or the ethylenic spacer has little effects on the compounds activity while modifying the terminal carboxylate function has a strong deleterious impact, except for the alcohol derivative (**Caf-CH$_2$OH**). It thus seems that a scaffold to inhibit GLIC currents should comprise an activated or weakly deactivated aromatic moiety linked to a polar function with proton-accepting abilities by a hydrophobic conjugate and planar arm.

pH-Dependence of the Inhibitory Effect. We tested the pH-dependence of the inhibitory effect for two representative compounds of the series, the titrable **Caf-COOH** and the nontitrable **Caf-CONHEt** (Figure 5). We found that monitoring inhibition in conditions of maximal activation at pH 4 produces a marked decrease in antagonists potency. Actually for both compounds, the limit of solubility did not allow reaching sufficiently high concentrations for measurement of complete dose–inhibition curves, precluding measurement of IC$_{50}$ and maximal inhibition. For **Caf-COOH** and **Caf-**
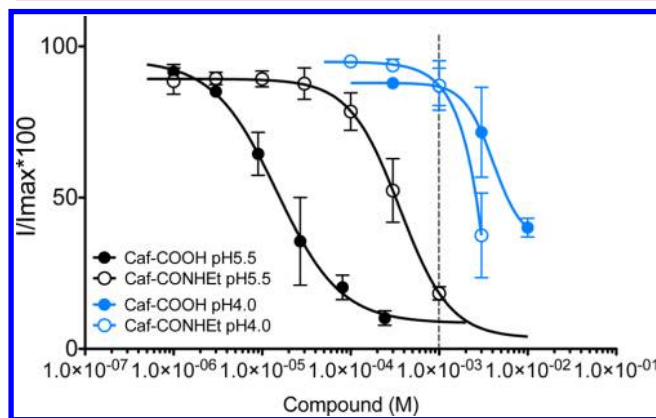
Figure 5. pH-dependence of the inhibition. Dose–inhibition curves of GLIC wild-type by the **Caf-COOH** and the **Caf-CONHEt** measured at pH 4.0 and 5.5. The dash line shows the limit for which the DMSO concentration can affect the data (0.1% DMSO inhibits GLIC currents).
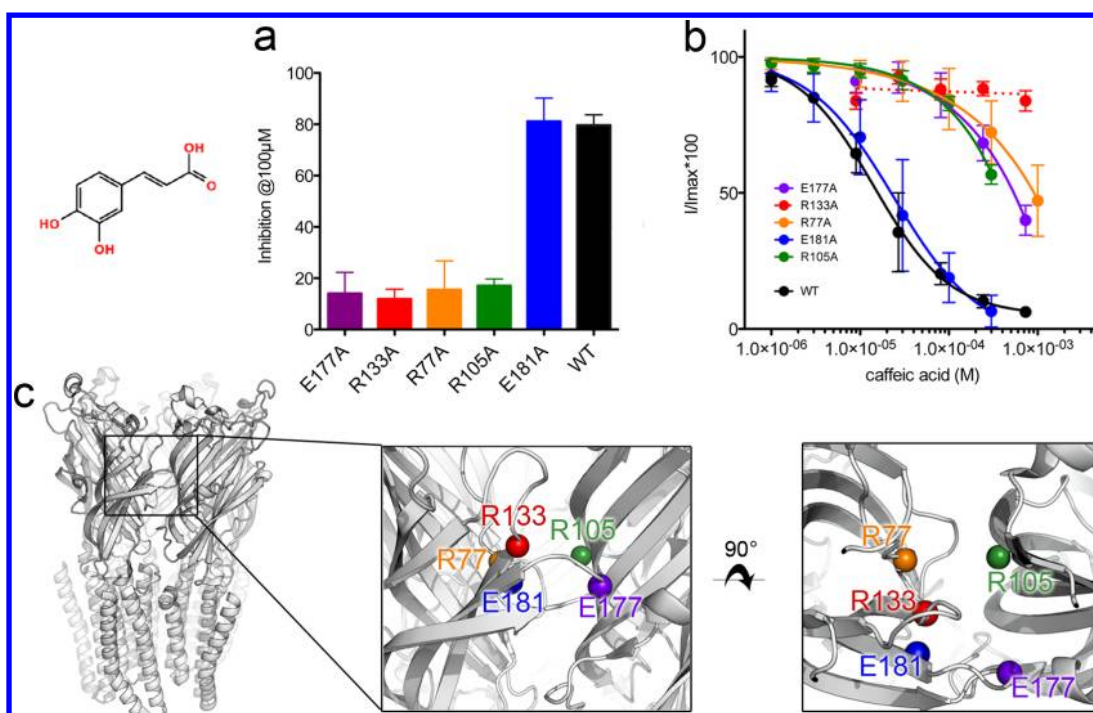
Figure 6. Effect of GLIC single mutations on the caffeic acid inhibition. (a) Maximal inhibition of GLIC WT and mutant obtained at pH 5.5 by 100 μM caffeic acid solution. (b) Concentration−inhibition curve of GLIC WT and mutants obtained at pH5.5. All points are mean $\pm$ sd with n (number of cells) $\geq$ 3. (c) The α-carbons of residues mutated into alanine are shown in spheres on GLIC structure seen in the side (left) and top (right) views.

CONHEt, the IC_{50}s shift from 16 and 295 μM at pH 5.5 to, assuming complete inhibition at maximal concentration, approximately 4000 and 2000 μM, respectively. Therefore, fully activated GLIC channels are more difficult to inhibit, further illustrating that caffeic derivatives act through an allosteric rather than through a channel blocking mechanism. Interestingly, the IC_{50} of **Caf-COOH** seems to increase much more than that of **Caf-CONHEt** upon acidification, suggesting that the protonated form of **Caf-COOH** might be less potent as an inhibitor than the conjugate base, **Caf-COO$^-$**.

The Caffeic Acid Inhibits GLIC near the Orthosteric Site. To investigate whether caffeic acid (**Caf-COOH**) binds nearby the orthosteric region of GLIC, we performed a series of single mutations on GLIC at positions known for their implication in the binding of orthosteric ligands in other pLGICs (Figure 6 and Supporting Information Table 1) and which would interact with the carboxylate group. We mutated titrable residues from the A-, B-, and C-loops in the principal subunit: Arg77 (hydrophobic residue in other pLGICs), Arg133 (aromatic residue in other pLGICs), and Glu177/Glu181, respectively. We also mutated a conserved arginine residue from $\beta6$ (E-loop) from the complementary subunit (Arg105) into alanine. Those single mutants exhibit wild-type properties regarding their proton sensitivity (pH$_{50}$ = 5.2 (pH allowing 50% of the maximal response), I_{max} = −5.9 μA, n_H = 2.0, Supporting Information Table 1).

Caffeic acid inhibition for the E181A mutant was similar to that observed for the wild-type (IC_{50} = 24.1 $\pm$ 3.4 μM, 80% inhibition at 100 μM). For R77A, R105A, and E177A, the concentration-inhibition shifts to higher concentrations by more than 10-fold (IC_{50} = 945, 420, and 506 μM, respectively, 15% inhibition at 100 μM, Figure 2), while for the R133A mutant, the caffeic acid has no more effect on the proton-elicited currents of GLIC even when applied at 1 mM. This

strongly suggests that the caffeic acid inhibitory site is located at the interface between subunit, close to residues 77, 105, 133, and 177.

IC_{50}s Are Correlated to a Posteriori in Silico Docking. To investigate a more realistic binding site for the evaluated compounds and interpret in a quantitative manner the structure−activity data, we ran another docking assay of the whole series of derivatives, this time using the intact open-channel X-ray structure of GLIC at 2.4 Å resolution[12] (PDB entry 4HFI). Because this structure does not exhibit cavities overlapping the other pLGICs orthosteric cavity, we considered a larger region (i.e., at more than 5 Å from nicotine), thus enlarging the previously defined three small cavities (Figure 7). At the bottom of the lower one that is below the C-loop, the 2.4 Å structure highlights the presence of an acetate molecule from the crystallization buffer, in tight interaction with Arg77 from the A-loop.[12] As the carboxylate group of the derivatives seemed to be determinant for their activity, we chose to target this particular cavity, which besides is surrounded by Arg77, Arg105, Arg133, and Glu181, to investigate the binding of our compounds (Figure 7). The docking was performed using leadit-1.3.0 (BioSolveIT, integrated version of FlexX), with a binding pocket from the list of residues closer than 8 Å from the acetate molecule. The dimer interface between chains C and D was used to dock 44 compounds, which had been converted into sdf format with openlabel 2.3.1 (http://openlabel.org). Ten poses were kept for each ligand, and the one yielding the best score was used for further analysis.

We compared the docking scores in this cavity with the measured IC_{50} (Figure 8) for the compounds with an IC_{50} <300 μM. Nineteen compounds could be docked and analyzed. Three compounds displayed poor correlation between their docking scores and measured IC_{50}. The 16 other ones yielded a satisfying correlation (Spearman nonparametric correlation

Figure 7. Docking pose of caffeic acid in the cavity that is predicted to bind acetate and ketamine. (a) Cavity lined by atoms within 5 Å of the acetate molecule in the GLIC structure (PDB entry 4HFI). The enlarged view shows the molecular docking of a caffeic acid molecule in this precise cavity. (b) Hydrophilic interactions predicted by the best docking pose. Dashes show interatoms distances <3 Å. (c) Residues of GLIC predicted to be at <5 Å of the caffeic acid. Residues in gray form a hydrophobic ring protecting the catechol moiety, hydrophilic residues in cyan contact the carboxylate and the hydroxyl moieties.

Figure 8. Correlation between docking scores in the acetate cavity and IC_{50} of the derivatives.

coefficient $r = 0.85$, $p < 0.0001$). The docking matched the structure−activity analysis: caffeic acid and other good inhibitors docked with good score into the targeted cavity (Figure 7), with the carboxylic acid positioned at the acetate binding site, facing the guanidinium residue of Arg77, at the same position as the acetate molecule in the GLIC structure (Supporting Information Figure 2). The negative charge of the carboxylate is also close to the side chains of Arg105 and Glu181. The aliphatic chain and the aromatic group are surrounded by five hydrophobic residues (Ile25, Phe42, Val79, Ile131, and Leu176). Those residues form a narrow tunnel that guides the two polar hydroxyl moieties in contact with Asn152 and the solvent.

This docking pose accounts for the structure−activity pattern, notably for the key role of the carboxylate function and the weak impact of the nature of the substituents of the phenyl part. Conversely, compounds without carboxylate and compounds presenting steric hindrance did not dock properly in agreement with their weak inhibitory effects (Figure 8). Altogether, these results suggest that the whole series binds to a common site, located in the orthosteric region of GLIC, except for the three outliers that have intermediate IC_{50} but a weak docking score. The outlier **Caf-CH₂-OH** docked similarly to the carboxylic acid series. The unfavorable score observed can be explained by the less stabilizing hydrogen interactions observed for **Caf-CH₂-OH** (one with Gly181 against three for carboxylate derivatives). Concerning the outliers **Cin-CH═C(COOH)₂** and **Napht-COOH**, these compounds do not display any pose into the acetate binding site. Two explanations are possible: first of all, we cannot exclude that these compounds target another binding site, also this could be due to the intrinsic limitations of the docking procedure that uses a rigid structure of the protein in an active conformation while we tried to bind antagonists. Indeed, the steric hindrance generated by the alkylidene malonate moiety or the naphthalene core, respectively, require some conformational reorganization of the hydrophobic tunnel to authorize their insertion.

Overall, this a posteriori docking allows proposing an extracellular binding site for the caffeic acid that is consistent with both structure−activity and mutagenesis data.

■ DISCUSSION AND CONCLUSIONS

In this study, we identified two cinnamic acid derivatives inhibiting GLIC at micromolar concentrations. Our combined mutational, structure−activity, and in silico docking analyses support that those compounds can bind in a pocket near the orthosteric site. Unexpectedly, our approach led to the discovery of antagonists and the docking assays were successful even if they were conducted on the open structure of GLIC. We have at present no answer to this paradox, but a possible interpretation is that those compounds would bind a closed-channel conformation with a higher affinity than the open-channel conformation (nonexclusive binding). In such a scheme, the orthosteric site would reorganize in an inactive state to allow a better interaction between the ligand and neighboring residues. Future experiments, notably by X-ray crystallography, are needed to challenge this hypothesis. Furthermore, this paradox could explain the relative low affinity of those inhibitors: one can imagine that a docking performed on a closed conformation of GLIC could lead to improved compounds with increased binding affinities.

Our analysis shows that mutations of titrable residues surrounding caffeic acid in the docking pose strongly decrease its inhibitory effect without significant changes in proton activation pharmacology. This suggests that protons and caffeic acid "binding" sites do not overlap completely. Furthermore, with the mutations presented in this work, we exclude some residues for being responsible by themselves for the proton sensitivity in the "orthosteric" site of GLIC. The proton activation site(s) are thus probably located in other parts of the ECD (at least in part), a question which remains open and difficult to tackle because proton activation of channels often involves clusters of charged residues as shown for ASICs or KcsA. In the case of GLIC, it is thus plausible that more than one single residue is involved, a cluster that could or could not

include those responsible for the caffeic binding. Most pLGICs are modulated by pH,[28−30] and some of them can directly be activated like GLIC by a change of extracellular proton concentration, such as the pHCl *Drosophila melanogaster*, which is activated at high pH,[31] or the PBO-5/6 from *C. elegans*, which is activated at low pH.[32] Nevertheless, the residues involved in these activations are also unknown and the sequence alignments show that their orthosteric site is completely different from that of GLIC.

Little is known about both the pharmacology and the physiological role of the prokaryotic pLGICs in bacteria. Concerning *Gloeobacter violaceus*, GLIC may constitute a proton sensor allowing the regulation of the proton gradients that are critical for cyanobacteria photosynthesis. The antagonists we identified are derived from cinnamic acid, which is part of the metabolism of phenylpropanoids, derived from phenylalanine and biosynthesized by plants. *Gloeobacter violaceus* is a photosynthetic bacterium, and even if its metabolism is not completely described, it is possible that this bacterium can synthesize cinnamic acid derivatives itself for quorum sensing or can be in contact with them in its native environment.

Anyhow, the cinnamic derivatives presented here will constitute useful tools to investigate the molecular mechanisms of signal transduction operating in GLIC. Indeed, several studies validated GLIC as a good model for understanding pLGICs properties: (i) GLIC functions as a ligand-gated ion channel that generates cationic currents upon proton binding,[13] (ii) the coupling of the ECD and the TMD in GLIC is similar to that occurring in eukaryotic pLGICs because the ECD of GLIC can be functionally coupled to the TMD of the α1GlyR,[14] (iii) GLIC is sensitive to classical allosteric modulators of eukaryotic pLGICs such as channel blockers,[33] alcohol,[34] or general anesthetics,[35] and the related binding sites were studied and identified by X-ray crystallography.[27,36−38] X-ray structures of GLIC in two conformations, an open-channel and locally closed form, allowed enrichment of our knowledge of the allosteric transitions of pLGICs[11,39] and gave clues to understand ion permeation.[12] The availability of large amount of GLIC also allowed biophysical investigations notably by EPR to probe the structural changes associated with desensitization.[40] However, due to the GLIC unusual mode of activation involving labile protons, the homology between GLIC and neurotransmitter-gated pLGICs with respect to the coupling of the agonist-binding site with the rest of the channel to open it through an allosteric transition can be questioned. In this context, our series of antagonists acting at the ECD thus provides new instruments to investigate the conformational changes occurring at this level as well as pharmacological tools to perform biophysical experiments and to trap additional closed-channel conformations of GLIC.

■ EXPERIMENTAL SECTION

Identification of Virtual Compounds in Virtual Libraries Using the InChiKey. Various commercial and academic libraries had been collected and installed (190 libraries covering appreciatively 7.7 million compounds, which 3D structures were calculated with protons). Global indexation of the compounds was built with their IUPAC International Chemical Identifiers (InChI).[41] To expedite the search of large number of compounds, the indices were preindexed hierarchically according their first characters. Use of two level of preindexation proved sufficient to extract efficiently dozens of thousands of compounds out of a meta base composed of multimillions of compounds.

Molecular Docking. The docking was performed using leadit-1.3.0 (BioSolveIT, integrated version of FlexX) with a binding pocket including the following list of residues closer than 8 Å from the acetate molecule (I25, F42, R77, F78, V79, R105, I131, R133, L176, and E181). The dimer interface between chains C and D was used to dock 44 compounds, which had been converted into sdf format with openlabel 2.3.1 (http://openlabel.org). Ten poses were kept for each ligand, and the one yielding the best score was used for further analysis.

Functional Assays. Chemicals, buffers, and media composition: The oocytes were obtained from the Center de Resources Biologiques—Rennes. Injected oocytes were incubated in Barth's medium (88 mM NaCl, 1 mM KCl, 2.4 mM NaHCO$_3$, 15 mM HEPES, 0.3 mM NaNO$_3$, 0.7 mM CaCl$_2$, 0.8 MgSO$_4$). The electrophysiological buffers contain 100 mM NaCl, 3 mM KCl, 1 mM CaCl$_2$, 1 mM MgCl$_2$, and 10 mM MES and are adjusted to the appropriate pH with HCl or NaOH. Stocks solutions of the compounds were prepared in DMSO or water at 0.5 or 1 M and were diluted directly in the buffer to the required concentration with pH adjusted to the indicated concentration. Compounds were prepared in a 1 M DMSO stock before being directly diluted in the recording solution. For acidic compounds, pH was adjusted by adding NaOH or pH 7.3 recording solution to reach a final pH of 5.5 or 4.0 depending on the conditions.

Electrophysiology recordings: Oocytes were prepared and recorded as previously described.[39] Traces were analyzed by Clampfit (Axon Instruments) or AxoGraph X and SigmaPlot 11 (Systat) or Plot. All currents were measured at −40 mV. Concentration-inhibition curves were fitted using:

$$\left(\frac{\text{Im } ax - I}{\text{Im } ax} \right) \times 100 = \left[1 - \frac{1}{1 + \left(\frac{\text{IC}_{50}}{[L]} \right)^{n\text{H}}} \right] \times 100$$

Chemistry. Commercial reagents were purchased at Sigma Aldrich and used without purification. Prior to use, acetone, THF, and MeOH were freshly distilled respectively from molecular sieves (3 Å), sodium/benzophenone, or Mg/I$_2$, while DCM was dried by means of a SP-1 stand alone solvent purification system apparatus (LC Technology Solutions Inc.). DMF was freshly distilled from CaH$_2$ at reduced pressure. All anhydrous reactions were carried out under argon atmosphere. Analytical thin layer chromatography was performed using glass plates precoated with silica gel 40 F$_{254}$ and was revealed by UV light. All flash chromatography separations were performed on silica gel (40−63 μm). Melting points were recorded on a melting point apparatus (Dr. Totoli) and were uncorrected. Infrared (IR) spectra were obtained as neat films. ^{1}H, ^{31}P, and ^{13}C spectra were recorded respectively at 300, 81, and 75 MHz. Deuterated solvent used as internal reference was specified for each compound. Purity of synthesized compounds was determined by RP-HPLC using a 150 mm × 2.1 mm (3.5 μm) XBridge C18 column: compounds were eluted in 20 min with a gradient from 95% MeCN/5% water/0.2% HCOOH to 5% MeCN/95% water/0.2%HCOOH.

General Procedure for the Synthesis of Ester Derivatives Caf-CO$_2$Me and Caf-CO$_2$Et. To a 0.5 M solution of caffeic acid **Caf-CO$_2$H** (1 equiv) in anhydrous alcohol was carefully added thionyl chloride (2.4 equiv). After refluxing for 1 h, the mixture was concentrated and the residue purified by column chromatography (cyclohexane/EtOAc 5/5) to yield the desired compound.

(E)-Methyl 3-(3,4-Dihydroxyphenyl)acrylate (Caf-CO$_2$Me). White solid (65% yield); R_f = 0.50 (cyclohexane/EtOAc 5/5); mp 160−162 °C (lit. 159 °C).[42] ^{1}H NMR (MeOD-d_4, 300 MHz) δ = 3.75 (s, 3H, CO$_2$CH$_3$), 6.25 (d, ^3J = 15.9 Hz, 1H, PhCH=CHCO$_2$), 6.79 (d, ^3J = 8.1 Hz, 1H, CHarom), 6.93 (dd, ^3J = 8.1 Hz, ^4J = 1.2 Hz, 1H, CHarom), 7.05 (d, ^4J = 1.1 Hz, 1H, CHarom), 7.54 (d, ^3J = 15.9 Hz, 1H, PhCH=CHCO$_2$). ^{13}C NMR (MeOD-d_4, 75 MHz) δ = 52.1 (CO$_2$CH$_3$), 114.9 + 115.2 + 116.5 + 123.0 (PhCH=CHCO$_2$ + 3 CHarom), 127.7 + 146.8 + 149.6 (3 Cqarom), 147.0 (PhCH= CHCO$_2$), 169.8 (CO$_2$). IR (cm^{-1}) ν_{max} = 3479, 2952, 2577, 1666,

1625, 1605, 1536, 1515, 1433, 1387, 1307, 1277, 1237, 1192, 1156, 1045, 969. HPLC purity (λ = 254 nm): 98% (retention time 12.4 min).

*(E)-Ethyl 3-(3,4-Dihydroxyphenyl)acrylate (**Caf-CO₂Et**).* White solid (85% yield); R_f = 0.45 (cyclohexane/EtOAc 5/5); mp 146–148 °C (lit. 149–151 °C).[21] ¹H NMR (acetone-d_6, 300 MHz) δ = 1.13 (t, ^3J = 7.2 Hz, 3H, CO₂CH₂CH_3), 4.05 (q, ^3J = 7.1 Hz, 2H, CO₂CH_2CH₃), 6.14 (d, ^3J = 15.9 Hz, 1H, PhCH=CHCO₂), 6.73 (d, ^3J = 8.4 Hz, 1H, CHarom), 6.90 (dd, ^3J = 8.1 Hz, ^4J = 1.8 Hz, 1H, CHarom), 7.03 (d, ^4J = 1.8 Hz, 1H, CHarom), 7.40 (d, ^3J = 15.9 Hz, 1H, PhCH=CHCO₂), 8.02 + 8.28 (2 bs, 2 × 1H, 2 OH). ¹³C NMR (acetone-d_6, 75 MHz) δ = 14.7 (CO₂CH₂CH₃), 60.6 (CO₂CH₂CH₃), 115.2 + 115.8 + 116.4 + 122.5 (PhCH=CHCO₂ + 3 CHarom), 127.7 + 146.3 + 148.7 (3 Cqarom), 145.6 (PhCH=CHCO₂), 167.5 (CO₂). IR (cm⁻¹) ν_{max} = 3430, 2960, 2581, 1658, 1610, 1596, 1515, 1453, 1307, 1281, 1219, 1173, 1118, 1051, 973. HPLC purity (λ = 254 nm): 99% (retention time 13.7 min).

*(E)-3-(3,4-Dihydroxyphenyl)-N-ethylacrylamide (**Caf-CONHEt**).* To a solution of caffeic acid **Caf-CO₂H** (108 mg, 0.60 mmol, 1 equiv) in DMF (1 mL), were added, at 0 °C, DIEA (110 µL, 0.63 mmol, 1 equiv), ethylamine 70 wt % in water (75 µL, 0.91 mmol, 1.1 equiv), then the solution of BOP (280 mg, 0.96 mmol, 1 equiv) in DCM (1 mL). After stirring at room temperature for 24 h, the mixture was concentrated and the residue poured into water and extracted three times with EtOAc. The combined organic layers were then washed with HCl 1 M and brine, dried over Na₂SO₄, filtered, and the filtrate concentrated. The residue was finally purified by column chromatography (cyclohexane/EtOAc 3/7) to yield **Caf-CONHEt** as a white solid (72 mg, 58% yield); R_f = 0.15 (cyclohexane/EtOAc 3/7); mp 178–181 °C (lit. 117–118 °C).[43] ¹H NMR (MeOD-d_4, 300 MHz) δ = 1.06 (t, ^3J = 7.4 Hz, 3H, CONHCH₂CH_3), 3.21 (q, ^3J = 7.2 Hz, 2H, CONHCH_2CH₃), 6.25 (d, ^3J = 15.6 Hz, 1H, PhCH=CHCON), 6.67 (d, ^3J = 8.4 Hz, 1H, CHarom), 6.79 (dd, ^3J = 8.1 Hz, ^4J = 1.8 Hz, 1H, CHarom), 6.91 (d, ^4J = 2.1 Hz, 1H, CHarom), 7.28 (d, ^3J = 15.6 Hz, 1H, PhCH=CHCON). ¹³C NMR (MeOD-d_4, 75 MHz) δ = 14.9 (CONHCH₂CH₃), 35.4 (CONHCH₂CH₃), 115.1 + 116.5 + 118.5 + 122.1 (PhCH=CHCON + 3 CHarom), 128.4 + 146.7 + 148.7 (3 Cqarom), 142.1 (PhCH=CHCON), 168.6 (CON). IR (cm⁻¹) ν_{max} = 3312, 2359, 1651, 1592, 1555, 1514, 1482, 1469, 1421, 1388, 1369, 1347, 1300, 1265, 1239, 1205, 1172, 1116, 992, 969. HPLC purity (λ = 320 nm): 95.5% (retention time 9.8 min).

*(E)-3-(3,4-Dihydroxyphenyl)acrylamide (**Caf-CONH₂**).* To a solution of caffeic acid **Caf-CO₂H** (200 mg, 1.1 mmol, 1 equiv) in DMF (1 mL), were added, at 0 °C, DIEA (195 µL, 1.1 mmol, 1 equiv), tritylamine (738 mg, 2.8 mmol, 2.5 equiv), and then the solution of BOP (475 mg, 1.1 mmol, 1 equiv) in DCM (2 mL). After stirring at room temperature for 96 h, the mixture was concentrated and the residue poured into water and extracted three times with EtOAc. The combined organic layers were then washed with HCl 1 M and brine, dried over Na₂SO₄, filtered, and the filtrate concentrated. The residue was finally purified by column chromatography (cyclohexane/EtOAc 5/5 to 3/7) to yield **Caf-CONHTr** as a white solid (132 mg, 28% yield); R_f = 0.35 (cyclohexane/EtOAc 5/5); mp 84–86 °C. ¹H NMR (MeOD-d_4, 300 MHz) δ = 7.20–7.30 (m, 20H, CHarom). ¹³C NMR (MeOD-d_4, 75 MHz) δ = 67.7 (CPh3), 115.4 + 116.5 + 119.3 + 122.3 (PhCH=CHCON + 3 CHarom), 127.9 (CHtrityl), 146.2 + 149.4 (2 Cqarom), 128.8 + 129.0 + 129.5 + 130.1 (CHtrityl), 142.7 (PhCH=CHCON), 168.7 (CONH). IR (cm-1) ν_{max} = 3473, 1595, 1488, 1444, 1285, 1201, 1180, 1117, 1032, 946. HPLC purity (λ = 320 nm): 70% (retention time 18.3 min). To a solution of **Caf-CONHTr** (66 mg, 0.16 mmol, 1 equiv) in anhydrous DCM (300 µL) was added TFA (600 µL). After stirring at room temperature for 3 h, addition of triethylsilane (75 µL, 0.47 mmol, 3 equiv) and further stirring at room temperature for 30 min, the mixture was concentrated and the residue purified by column chromatography (EtOAc 100) to yield **Caf-CONH₂** as a white solid (19 mg, 68% yield); R_f = 0.45 (EtOAc 100); mp 165–169 °C. ¹H NMR (MeOD-d_4, 300 MHz) δ = 6.40 (d, 3J = 15.6 Hz, 1H, PhCH=CHCON), 6.76 (dd, 3J = 8.1 Hz, 4J = 1.5 Hz, 1H, CHarom), 6.91 (d, 3J = 8.4 Hz, 1H, CHarom), 7.01 (d, 4J = 1.8 Hz, 1H, CHarom), 7.41 (d, 3J = 15.9 Hz, 1H, PhCH=CHCON). ¹³C

NMR (MeOD-d_4, 75 MHz) δ = 115.1 + 116.5 + 117.8 + 122.3 (PhCH=CHCON + 3 CHarom), 128.2 + 146.8 + 149.0 (3 Cqarom), 143.4 (PhCH=CHCON), 171.7 (CONH). IR (cm-1) ν_{max} = 3330, 1680, 1649, 1626, 1564, 1528, 1451, 1207, 1196, 1137, 1109, 969. HRMS calcd for C₉H₉NO₃ ([M + Na]⁺), 202.0480; found, 202.0486. HPLC purity (λ = 320 nm): 98% (retention time 7.1 min).

*3-(3,4-Dihydroxyphenyl)propanoic Acid (**α,β-diH-Caf-CO₂H**).* To a solution of **Caf-CO₂H** (81 mg, 0.45 mmol, 1 equiv) in MeOH (4 mL) was added catalytic amount of Pd/C. After stirring at room temperature overnight under an hydrogen atmosphere (1 atm), the mixture was filtered over Celite, washed with MeOH, and the filtrate concentrated to yield **α,β-diH-Caf-CO₂H** as a white solid (80.5 mg, 99% yield); R_f = 0.21 (cyclohexane/EtOAc 5/5); mp 134–136 °C (lit. 137–139 °C).[44] ¹H NMR (MeOD-d_4, 300 MHz) δ = 2.42 (t, ^3J = 7.5 Hz, 2H, PhCH₂-CH_2CO₂), 2.65 (t, ^3J = 7.7 Hz, 2H, PhCH_2-CH₂CO₂), 6.42 (dd, ^3J = 7.8 Hz, ^4J = 1.5 Hz, 1H, CHarom), 6.56 (d, ^4J = 1.8 Hz, 1H, CHarom), 6.57 (d, ^3J = 8.4 Hz, 1H, CHarom). ¹³C NMR (MeOD-d_4, 75 MHz) δ = 31.5 (PhCH₂-CH₂CO₂), 37.4 (PhCH₂-CH₂CO₂), 116.4 + 116.5 + 120.6 (3 CHarom), 133.9 + 144.5 + 146.2 (3 Cqarom). IR (cm⁻¹) ν_{max} = 3300, 1713, 1604, 1518, 1444, 1362, 1284, 1194, 1149, 1113. HPLC purity (λ = 240 nm) > 99% (retention time 9.2 min).

*(E)-4-(3-Hydroxyprop-1-enyl)benzene-1,2-diol (**Caf-CH₂OH**).* To a solution of LiAlH₄ (31 mg, 0.8 mmol, 1.9 equiv) in anhydrous THF (4 mL) was added dropwise a solution of benzyl chloride (94 µL, 0.8 mmol, 1.9 equiv) in anhydrous THF (1 mL), and the mixture was stirred at room temperature for 30 min to allow formation of AlH₃. To this solution was added dropwise a solution of **Caf-CO₂Me** (83 mg, 0.4 mmol, 1 equiv) in anhydrous THF (1 mL). After further stirring at room temperature for 5 h, the mixture was successively treated with NaHCO₃ 5% (10 mL) and HCl 1 M (10 mL) then extracted with DCM (3 × 10 mL). The combined organic layers were washed with brine (15 mL), dried over Na₂SO₄, filtered, and concentrated. The residue was finally purified by column chromatography (cyclohexane/EtOAc 5/5) to yield **Caf-CH₂OH** as a brownish solid (25 mg, 35% yield); R_f = 0.15 (cyclohexane/EtOAc 5/5); mp 147 °C (lit. 144–145 °C).[45] ¹H NMR (MeOD-d_4, 300 MHz) δ = 16 (dd, ^2J = 1.5 Hz, ^3J = 6.0 Hz, 2H, CH_2OH), 6.11 (td, ^3J = 6.0 Hz, ^3J = 15.6 Hz, 1H, PhCH=CHCH₂), 6.43 (d, ^3J = 15.6 Hz, 1H, PhCH=CHCH₂), 6.72 (m, 2H, CHarom), 6.87 (d, ^4J = 1.5 Hz, 1H, CHarom). ¹³C NMR (MeOD-d_4, 75 MHz) δ = 64.0 (CH₂OH), 114.0 + 116.3 + 119.9 + 126.7 (PhCH=CHCH₂ + 3 CHarom), 130.7 + 146.4 + 146.4 (3 Cqarom), 132.2 (PhCH=CHCH₂). IR (cm⁻¹) ν max 3600–3300, 2928, 1652, 1591, 1458, 1416, 1058, 968. HPLC purity (λ = 254 nm): 86% (retention time 8.8 min).

*(E)-N-Methoxycinnamamide (**Cin-CONHOMe**).* To a solution of **Cin-CO₂H** (300 mg, 2 mmol, 1 equiv) in anhydrous DCM (10 mL) was added dropwise thionyl chloride (365 µL, 5 mmol, 2.5 equiv). After refluxing for 2 h and cooling, the mixture was concentrated and diluted with anhydrous DCM (20 mL). O-Methylhydroxylamine hydrochloride (126 mg, 2.3 mmol, 1.1 equiv) and pyridine (390 µL, 4.9 mmol, 2.4 equiv) were added at 0 °C. After stirring at rt overnight, the reactive medium was washed with water, and the organic layer was then dried over Na₂SO₄, filtered, and the filtrate concentrated. The residue was finally purified by column chromatography (cyclohexane/EtOAc 5/5) to yield **Cin-CONHOMe** as a white solid (250 mg, 70% yield); R_f = 0.30 (cyclohexane/EtOAc 5/5); mp = 87–90 °C (lit. 93–95 °C).[25] ¹H NMR (CDCl₃, 300 MHz) δ 3.75 (s, 3H, OCH_3), 6.56 (m, 1H, PhCH=CHCO), 7.20 (m, 4H, CHarom), 7.39 (m, 1H, CHarom), 7.65 (d, ^3J = 15.6 Hz, 1H, PhCH=CHCO), 10.70 (bs, 1H, NH). ¹³C NMR (CDCl₃, 75 MHz) δ 64.3 (OCH₃), 117.3 (PhCH=CHCO), 127.9 + 128.8 + 129.9 (3 CHarom), 134.7 (Cqarom), 144.8 (PhCH=CHCO), 164.7 (CO). IR (cm⁻¹) ν max 3130, 1649, 1617, 1522, 1342, 1220, 1059, 972, 929. HPLC purity (λ = 254 nm): 98% (retention time 12.3 min).

*2-Benzylidenemalonic Acid (**Cin-(CO₂H)₂**).* A mixture of benzaldehyde (200 µL, 2.0 mmol, 1 equiv), malonic acid (206 mg, 2.0 mmol, 1 equiv), and L-proline (24 mg, 0.2 mmol, 0.1 equiv) was heated at 95 °C for 2 h then cooled and diluted in DCM. The organic layer was washed with HCl 1M, and then the aqueous layer was extracted with

DCM. The combined organic layers were dried over Na_2SO_4, filtered, and the filtrate concentrated. The residue was finally recrystallized in DCM to yield the desired compound **Cin-$(CO_2H)_2$** (152 mg, 40% yield); R_f < 0.05 (DCM/EtOH 9/1); mp =188−190 °C (lit. 191 °C).[46] ^{1}H NMR (MeOD-d_4, 300 MHz) δ = 5.73 (bs, 2H, 2 CO*OH*), 7.40 (m, 3H, C*H*arom), 7.58 (m, 2H, C*H*arom), 7.70 (s, 1H, Ph*CH*= C$(CO_2H)_2$). ^{13}C NMR (MeOD-d_4, 75 MHz) δ = 128.6 (PhCH= C$(CO_2H)_2$), 130.0 + 130.6 + 131.8 (3 *CH*arom), 134.3 (*Cq*arom), 146.6 (Ph*CH*=C$(CO_2H)_2$), 167.3 + 170.8 (2 *CO*). IR (cm^{-1}) ν_{max} = 2720, 1713, 1695, 1672, 1424, 1282, 1251, 909; HPLC purity (λ = 254 nm): 96% (retention time 11.2 min).

(E)-2-(3-Phenylallylidene)malonic Acid (**Cin-CH=C$(CO_2H)_2$**). To a solution of cinnamaldehyde (150 μL, 1.2 mmol, 1 equiv) in pyridine (0.5 mL) was added malonic acid (273 mg, 2.6 mmol, 2.2 equiv) and piperidine (24 μL, 0.24 mmol, 0.2 equiv). After ultrasonic irradiation for 3 h, the mixture was cooled, poured into cooled HCl 2 M (15 mL), and filtered to yield the desired compound **Cin-CH=C$(CO_2H)_2$** as a yellow solid (235 mg, 90% yield); mp 186−188 °C (lit. 183−186 °C).[47] ^{1}H NMR (MeOD-d_4, 300 MHz) δ = 7.29 (d, J = 14.5 Hz, 1H, CH=), 7.41 (m, 3H, C*H*arom), 7.55−7.65 (m, 2H, C*H*arom), 7.79 (dd, J = 11.7 and 14.5 Hz, CH=), 7.87 (d, J = 11.6 Hz, 1H, CH=). ^{13}C NMR (DMSO-d_6, 75 MHz) δ = 122.1 (*Cq*(COOH)$_2$), 125.2 (*CH*=), 131.6 + 130.1 + 129.2 (*CH*arom), 137.1 (*Cq*arom), 150.9 + 148.7 (CH=), 169.0 (*CO_2H*). IR (cm^{-1}) ν max 3189, 3091, 1968, 1732, 1719, 1601, 1577, 1414, 1174, 995. HPLC purity (λ = 320 nm): 99% (retention time 13.1 min).

ASSOCIATED CONTENT

Ⓢ Supporting Information

Peptide sequence alignments of A-, B-, and C- loops for several pLGICs, relative position of the caffeic acid from the docking assay and the acetate binding site in the GLIC structure, electrophysiological properties of GLIC mutants, and ^{1}H and ^{13}C NMR spectra of synthesized compounds. This material is available free of charge via the Internet at http://pubs.acs.org.

AUTHOR INFORMATION

Corresponding Author

*For T.E.M.: E-mail, terez@pasteur.fr; phone, (33)1 40 61 34 75; fax, (33)1 45 68 87 19. For P.-J.C.: E-mail, pjcorrin@ pasteur.fr; phone, (33)1 40 61 31 02; fax, (33)1 45 68 88 36. For D.J.: E-mail: delphine.joseph@u-psud.fr; phone, (33)1 46 83 57 30. Fax: (33)1 46 83 57 52.

Notes

The authors declare no competing financial interest.

ACKNOWLEDGMENTS

ABBREVIATIONS USED

AChBP, acetylcholine binding protein; ASIC, acid-sensing ion channel; ECD, extracellular domain; ELIC, *Erwinia chrysanthemi* ligand-gated ion channel; GABAR, γ-aminobutyric acid receptor; GLIC, *Gloeobacter violaceus* ligand-gated ion channel; GlyR, glycine receptor; GluCl, glutamate chloride channel; HEPES, 4-(2-hydroxyethyl)-1-piperazineethanesulfonic acid; 5-HT$_3$R, 5-hydroxytryptamine receptor; KEGG, Kyoto Encyclopedia of Genes and Genomes; KcsA, potassium crystallographically sited activation channel; Ls-AChBP, *Lymnaea stagnalis* acetylcholine binding protein; MES, 2-(*N*-morpholino)ethanesulfonic acid; nAChR, nicotinic acetylcholine receptor; PBO, posterior body; pHCl, pH-sensitive chloride channel; pH$_{xx}$, pH allowing the recording of xx% of the GLIC proton-elicited maximal current; pLGIC, pentameric ligand gated ion channels; TMD, transmembrane domain

REFERENCES

(1) Corringer, P.-J.; Poitevin, F.; Prevost, M. S.; Sauguet, L.; Delarue, M.; Changeux, J.-P. Structure and Pharmacology of Pentameric Receptor Channels: From Bacteria to Brain. *Structure* **2012**, *20*, 941−956.

(2) Tasneem, A.; Iyer, L.; Jakobsson, E.; Aravind, L. Identification of the Prokaryotic Ligand-Gated Ion Channels and Their Implications for the Mechanisms and Origins of Animal Cys-Loop Ion Channels. *Genome Biol.* **2004**, *6*, R4.

(3) Hibbs, R. E.; Gouaux, E. Principles of Activation and Permeation in an Anion-Selective Cys-Loop Receptor. *Nature* **2011**, *474*, 54−60.

(4) Zimmermann, I.; Dutzler, R. Ligand Activation of the Prokaryotic Pentameric Ligand-Gated Ion Channel ELIC. *PLoS Biol.* **2011**, *9*, e1001101.

(5) Pan, J.; Chen, Q.; Willenbring, D.; Yoshida, K.; Tillman, T.; Kashlan, O. B.; Cohen, A.; Kong, X.-P.; Xu, Y.; Tang, P. Structure of the Pentameric Ligand-Gated Ion Channel ELIC Co-Crystallized with its Competitive Antagonist Acetylcholine. *Nature Commun.* **2012**, *3*, 714.

(6) Rucktooa, P.; Smit, A. B.; Sixma, T. K. Insight in nAChR Subtype Selectivity from AChBP Crystal Structures. *Biochem. Pharmacol.* **2009**, *78*, 777−787.

(7) Zhong, W.; Gallivan, J. P.; Zhang, Y.; Li, L.; Lester, H. A.; Dougherty, D. A. From ab Initio Quantum Mechanics to Molecular Neurobiology: A Cation−π Binding Site in the Nicotinic Receptor. *Proc. Natl. Acad. Sci. U. S. A.* **1998**, *95*, 12088−12093.

(8) Pless, S. A.; Millen, K. S.; Hanek, A. P.; Lynch, J. W.; Lester, H. A.; Lummis, S. C. R.; Dougherty, D. A. A Cation−π Interaction in the Binding Site of the Glycine Receptor is Mediated by a Phenylalanine Residue. *J. Neurosci.* **2008**, *28*, 10937−10942.

(9) Lummis, S. C. R.; Beene, D. L.; Harrison, N. J.; Lester, H. A.; Dougherty, D. A. Cation−π Binding Interaction with a Tyrosine in the Binding Site of the GABAc Receptor. *Chem. Biol.* **2005**, *12*, 993−997.

(10) Beene, D. L.; Brandt, G. S.; Zhong, W.; Zacharias, N. M.; Lester, H. A.; Dougherty, D. A. Cation−π Interactions in Ligand Recognition by Serotonergic (5-HT$_{3A}$) and Nicotinic Acetylcholine Receptors: The Anomalous Binding Properties of Nicotine. *Biochemistry* **2002**, *41*, 10262−10269.

(11) Bocquet, N.; Nury, H.; Baaden, M.; Le Poupon, C.; Changeux, J.-P.; Delarue, M.; Corringer, P.-J. X-Ray Structure of a Pentameric Ligand-Gated Ion Channel in an Apparently Open Conformation. *Nature* **2009**, *457*, 111−114.

(12) Sauguet, L.; Poitevin, F.; Murail, S.; Van Renterghem, C.; Moraga-Cid, G.; Malherbe, L.; Thompson, A. W.; Koehl, P.; Corringer, P.-J.; Baaden, M.; Delarue, M. Structural Basis for Ion Permeation Mechanism in Pentameric Ligand-Gated Ion Channels. *EMBO J.* **2013**, *32*, 728−741.

(13) Bocquet, N.; Prado De Carvalho, L.; Cartaud, J.; Neyton, J.; Le Poupon, C.; Taly, A.; Grutter, T.; Changeux, J.-P.; Corringer, P.-J. A Prokaryotic Proton-Gated Ion Channel from the Nicotinic Acetylcholine Receptor Family. *Nature* **2007**, *445*, 116−119.

(14) Duret, G.; Van Renterghem, C.; Weng, Y.; Prevost, M.; Moraga-Cid, G.; Huon, C.; Sonner, J. M.; Corringer, P.-J. Functional Prokaryotic−Eukaryotic Chimera from the Pentameric Ligand-Gated Ion Channel Family. *Proc. Natl. Acad. Sci. U. S. A.* **2011**, *108*, 12143−12148.

(15) Ho, B. K.; Gruswitz, F. HOLLOW: Generating Accurate Representations of Channel and Interior Surfaces in Molecular Structures. *BMC Struct. Biol.* **2008**, *8*, 49.

(16) Sadowski, J.; Gasteiger, J.; Klebe, G. J. The Generation and Use of Large 3D Databases in Drug Discovery. *Chem. Inf. Comput. Sci.* **1994**, *34*, 1000−1008.

(17) Schwab, C. H. Conformations and 3D Pharmacophore Searching. *Drug Discovery Today: Technol.* **2010**, *7*, e245−e253.

(18) Eswar, N.; Webb, B.; Marti-Renom, M. A.; Madhusudhan, M. S.; Eramian, D.; Shen, M.-Y.; Pieper, U.; Sali, A. Comparative Protein Structure Modeling Using MODELLER. *Curr. Protoc. Bioinform.* **2006**, 5.6.1−5.6.30.

(19) Gastreich, M.; Lilienthal, M.; Briem, H.; Claussen, H. Ultrafast de novo Docking Combining Pharmacophores and Combinatorics. *J. Comput.-Aided Mol. Des.* **2006**, *20*, 717−734.

(20) InChiKeys are 25 characters codes, derived by mathematical hashing of the IUPAC InChi (International Chemical Identifier; IUPAC, 5 September 2007), which describes chemical topology of compounds by a unique string of character.

(21) Uwai, K.; Osanai, Y.; Imaizumi, T.; Kanno, S.-I.; Takeshita, M.; Ishikawa, M. Inhibitory Effect of the Alkyl Side Chain of Caffeic Acid Analogues on Lipopolysaccharide-Induced Nitric Oxide Production in RAW264.7 Macrophages. *Bioorg. Med. Chem.* **2008**, *16*, 7795−7803.

(22) Fu, J.; Cheng, K.; Zhang, Z.-M.; Fang, R.-Q.; Zhu, H.-L. Synthesis, Structure and Structure−Activity Relationship Analysis of Caffeic Acid Amides as Potential Antimicrobials. *Eur. J. Med. Chem.* **2010**, *45*, 2638−2643.

(23) Theodorou, V.; Karkatsoulis, A.; Kinigopulou, M.; Ragoussis, V.; Skobridis, K. Tritylamine as an Ammonia Synthetic Equivalent: Preparation of Primary Amides. *ARKIVOC* **2009**, 277−287.

(24) Wang, X.; Li, X.; Xue, J.; Zhao, Y.; Zhang, Y. A Novel and Efficient Procedure for the Preparation of Allylic Alcohols from α,β-Unsaturated Carboxylic Esters Using $LiAlH_4$/BnCl. *Tetrahedron Lett.* **2009**, *50*, 413−415.

(25) Miyata, O.; Koizumi, T.; Asai, H.; Iba, R.; Naito, T. Imino 1,2-Wittig Rearrangement of Hydroximates and its Application to Synthesis of Cytoxazone. *Tetrahedron* **2004**, *60*, 3893−3914.

(26) Karade, N. N.; Gampawar, S. V.; Shinde, S. V.; Jadhav, W. N. L-Proline Catalyzed Solvent-Free Knoevenagel Condensation for the Synthesis of 3-Substituted Coumarins. *Chin. J. Chem.* **2007**, *25*, 1686−1689.

(27) Pan, J.; Chen, Q.; Willenbring, D.; Mowrey, D.; Kong, X.-P.; Cohen, A.; Divito, C. B.; Xu, Y.; Tang, P. Structure of the Pentameric Ligand-Gated Ion Channel GLIC Bound with Anesthetic Ketamine. *Structure* **2012**, *20*, 1463−1469.

(28) Mercik, K.; Pytel, M.; Cherubini, E.; Mozrzymas, J. W. Effect of Extracellular pH on Recombinant $\alpha 1\beta 2\gamma 2$ and $\alpha 1\beta 2$ $GABA_A$ Receptors. *Neuropharmacology* **2006**, *51*, 305−314.

(29) Abdrakhmanova, G.; Cleemann, L.; Lindstrom, J.; Morad, M. Differential Modulation of $\beta 2$ and $\beta 4$ Subunits of Human Neuronal Nicotinic Acetylcholine Receptors by Acidification. *Mol. Pharmacol.* **2004**, *66*, 347−355.

(30) Chen, Z.; Dillon, G. H.; Huang, R. Molecular Determinants of Proton Modulation of Glycine Receptors. *J. Biol. Chem.* **2004**, *279*, 876−883.

(31) Mounsey, K. E.; Dent, J. A.; Holt, D. C.; McCarthy, J.; Currie, B. J.; Walton, S. F. Molecular Characterization of a pH-Gated Chloride Channel from *Sarcoptes scabiei*. *Invertebr. Neurosci.* **2007**, *7*, 149−156.

(32) Beg, A. A.; Ernstrom, G. G.; Nix, P.; Davis, M. W.; Jorgensen, E. M. Protons Act as a Transmitter for Muscle Contraction in *C. elegans*. *Cell* **2008**, *132*, 149−160.

(33) Alqazzaz, M.; Thompson, A. J.; Price, K. L.; Breitinger, H.-G.; Lummis, S. C. R. Cys-Loop Receptor Channel Blockers Also Block GLIC. *Biophys. J.* **2011**, *101*, 2912−2918.

(34) Howard, R. J.; Murail, S.; Ondricek, K. E.; Corringer, P.-J.; Lindahl, E.; Trudell, J. R.; Harris, R. A. Structural basis for alcohol modulation of a pentameric ligand-gated ion channel. *Proc. Nat. Acad. Sci. U. S. A.* **2011**, *108*, 12149−12154.

(35) Weng, Y.; Yang, L.; Corringer, P.-J.; Sonner, J. M. Anesthetic Sensitivity of the *Gloeobacter violaceus* Proton-Gated Ion Channel. *Anesth. Analg.* **2010**, *110*, 59−63.

(36) Nury, H.; Van Renterghem, C.; Weng, Y.; Tran, A.; Baaden, M.; Dufresne, V.; Changeux, J.-P.; Sonner, J. M.; Delarue, M.; Corringer, P.-J. X-Ray Structures of General Anaesthetics Bound to a Pentameric Ligand-Gated Ion Channel. *Nature* **2011**, *469*, 428−431.

(37) Hilf, R. J. C.; Bertozzi, C.; Zimmermann, I.; Reiter, A.; Trauner, D.; Dutzler, R. Structural Basis of Open Channel Block in a Prokaryotic Pentameric Ligand-Gated ion Channel. *Nature Struct. Mol. Biol.* **2010**, *17*, 1330−1336.

(38) Sauguet, L.; Howard, R. J.; Malherbe, L.; Lee, U. S.; Corringer, P.-J.; Harris, R. A.; Delarue, M. Structural Basis for Potentiation by Alcohols and Anesthetics in a Ligand-gated Ion Channel. *Nature Commun.* **2013**, *4*, 1697, doi 10.1038/ncomms2682.

(39) Prevost, M. S.; Sauguet, L.; Nury, H.; Van Renterghem, C.; Huon, C.; Poitevin, F.; Baaden, M.; Delarue, M.; Corringer, P.-J. A Locally Closed Conformation of a Bacterial Pentameric Proton-gated Ion Channel. *Nature Struct. Mol. Biol.* **2012**, *19*, 642−649.

(40) Velisetty, P.; Chakrapani, S. Desensitization Mechanism in Prokaryotic Ligand-Gated Ion Channel. *J. Biol. Chem.* **2012**, *287*, 18467−18477.

(41) McNaught, A. The IUPAC International Chemical Identifier:-InChI. *Chemistry Int.* **2006**, *28*, 12−15.

(42) Bernini, R.; Barontini, M.; Mosesso, P.; Pepe, G.; Willför, S . M.; Sjöholm, R. E.; Eklund, P. C.; Saladino, H. A Selective De-*O*-methylation of Guaiacyl Lignans to Corresponding Catechol Derivatives by 2-Iodoxybenzoic Acid (IBX). The Role of the Catechol Moiety on the Toxicity of Lignans. *Org. Biomol. Chem.* **2009**, *7*, 2367−2377.

(43) Fu, J.; Cheng, K.; Zhang, Z.-M.; Fang, R.-Q.; Zhu, H.-L. Synthesis, Structure and Structure−Activity Relationship Analysis of Caffeic Acid Amides as Potential Antimicrobials. *Eur. J. Med. Chem.* **2010**, *45*, 2638−2643.

(44) Deng, L.; Sundiyal, S.; Rubio, V.; Shi, Z.-Z.; Song, Y. Coordination Chemistry Based Approach to Lipophilic Inhibitors of 1-Deoxy-D-xylulose-5-phosphate Reductoisomerase. *J. Med. Chem.* **2009**, *52*, 6539−6542.

(45) Freudenberg, K.; Heel, W. Dioxy- und Trioxy-zimtalalkohol. *Chem. Ber.* **1953**, *86*, 190−196.

(46) Sharma, Y. O.; Degani, M. S. CO_2 Absorbing Cost-effective Ionic Liquid for Synthesis of Commercially Important Alpha Cyanoacrylic Acids: A Safe Process for Activation of Cyanoacetic Acid. *Green Chem.* **2009**, *11*, 526−530.

(47) Gardner, P. D.; Horton, W. J.; Thompson, G.; Twelves, R. R. A New Approach to δ-Phenylvaleric Acids. *J. Am. Chem. Soc.* **1952**, *74*, 5527−5529.